Ultrafast Optical Kerr Effect in Liquids and Solids

Roberto Righini

In the optical Kerr effect, the electric field of light incident on a transparent sample induces an anisotropic refractive index, which is measured by its effect on the passage of a second light beam. The advent of lasers powerful enough to generate a measurable effect, and which can be pulsed on femtosecond time scales, has made the optical Kerr effect into a practical technology for investigating the molecular structure and interactions of condensed systems such as pure liquids, liquid solutions, and plastic crystals.

A strong electric field applied to a liquid transparent sample induces an optical anisotropy in the medium. The material is thus characterized by two different values of the refractive index $n_{\perp}$ and $n_{\parallel}$, where parallel and perpendicular refer to the direction of the applied field **E**. If the electric field is applied in, say, the y direction, a light beam propagating along z and linearly polarized in the xy plane experiences a phase difference Φ between the parallel and perpendicular components (birefringence). This birefringence is proportional to $(n_{\parallel} - n_{\perp})$ that, in turn, depends on the square of the applied field

$$\Phi = \frac{2\pi\ell}{\lambda}(n_{\parallel} - n_{\perp}) = 2\pi\ell B E^2 \qquad (1)$$

where B is a constant, and ℓ is the path length traveled in the sample by the light of wavelength λ. This is the essence of the Kerr effect, first discovered and described by Kerr around the middle of 19th century.

Consider now that the light beam incident on a liquid sample with intensity I_0 passes through two crossed polarizers, placed before and after the sample, respectively. In the absence of any electrically induced birefringence, no light is detected after the second polarizer. When the electric field is switched on, the birefringence induced in the sample causes a partial depolarization of the light so that an intensity I is detected after the second polarizer. The observed intensity depends on the induced phase shift Φ according to

$$I = I_0 \sin^2 \Phi/2 \qquad (2)$$

For small values of Φ the transmitted intensity is then proportional to the square of the phase difference. In the optical Kerr effect (OKE) the field inducing the birefringence is the oscillating electric field of the electromagnetic radiation (*1*). Although predicted in earlier times, the OKE became measurable only after the advent of intense laser sources. In an OKE experiment, two linearly polarized laser beams are then used according to the scheme of Fig. 1. Four electric fields are involved: the electric field of the incident beam probing the birefringence, that of the light emerging from the second polarizer, and the field of the beam inducing the birefringence, which, according to Eq. 1, acts at the second power. The OKE is then part of the large family of four-wave mixing processes, that is, of the nonlinear optical effects that can be described in terms of the third-order material polarization (*2*). The time-dependent polarization $\mathbf{P}(t)$ can be expanded in a power series

$$\mathbf{P}(t) = \mathbf{P}^{(0)}(t) + \mathbf{P}^{(1)}(t) + \mathbf{P}^{(2)}(t) + \mathbf{P}^{(3)}(t) + \ldots \qquad (3)$$

in which $\mathbf{P}^{(1)}$ is proportional to the applied electric field **E**, $\mathbf{P}^{(2)}$ to the second power of **E**, and so on. The term of interest in our case is the third-order polarization, whose general expression is

$$\mathbf{P}_i^{(3)}(t) = \int_{-\infty}^{t} dt' \int_{-\infty}^{t'} dt'' \int_{-\infty}^{t''} dt''' \chi_{ijkl}^{(3)}(t,t',t'',t''')\mathbf{E}_j(t')\mathbf{E}_k(t'')\mathbf{E}_l(t''') \qquad (4)$$

The relevant quantity in Eq. 4 is the third-order electric susceptibility of the sample $\chi_{ijkl}^{(3)}$; the subscripts refer to the polarization directions of the electric fields involved in the process. The three electric fields on the right side of Eq. 4, corresponding to the incident probe beam and to the two exciting beams, are considered to be applied at the times t', t'', and t''', respectively. The time-dependent third-order polarization on the left side of the same equation acts as the source term for the light (polarized along i) that is observed in an OKE experiment at the end of the optical chain shown in Fig. 1. The direction of propagation of the light is indicated with 3, and 1 and 2 indicate the other two orthogonal directions of a laboratory fixed frame. Simple geometrical considerations on the polarization geometry of the experiment described in Fig. 1 give the value for the $\mathbf{P}_i^{(3)}$ component of Eq. 4 of

$$\mathbf{P}_i^{(3)} = \frac{\sqrt{2}}{2}(\mathbf{P}_1^{(3)} - \mathbf{P}_2^{(3)}) \qquad (5)$$

which, in turn, can be expressed in terms of the susceptibility tensor as

$$\mathbf{P}_i^{(3)} \propto (\chi_{1111}^{(3)} - \chi_{1122}^{(3)})\mathbf{E}^2 \qquad (6)$$

The induced birefringence can thus be written as

$$\delta n = n_{\parallel} - n_{\perp} = \frac{\pi}{n} \int_{-\infty}^{t} dt'[\chi_{1111}^{(3)} - \chi_{1122}^{(3)}]|\mathbf{E}(t')|^2 \qquad (7)$$

In a time-resolved experiment the electromagnetic fields are applied in the form of light pulses, as short as a few tens of femtoseconds (10^{-15} s). The different times that appear in Eq. 4 have then a full physical meaning. The experiment consists of an intense excitation pulse I_e that induces the birefringence at a given time, thus setting the relative time origin of the experiment, and of a probe pulse I_p that reaches the same volume of the sample with a variable delay τ, thus probing the residual birefringence. The intensity of the probe pulse transmitted through the second polarizer, as a function of the time delay is then

$$S(\tau) \propto \int_{-\infty}^{\infty} dt I_p(t-\tau)[\delta n(t)]^2 \propto \int_{-\infty}^{\infty} dt I_p(t-\tau)\left[\int_{-\infty}^{t} dt' R(t-t') I_e(t')\right]^2 \qquad (8)$$

where the response function of the system is given by

$$R(t) = \chi_{1111}^{(3)}(t) - \chi_{1122}^{(3)}(t) \qquad (9)$$

The key point of the transient OKE experiment, the characteristic that makes it possible to extract information on the dynamics of the material at a microscopic level, relies on the structure itself of the third-order susceptibility. There are two contributions (*2*) to the response of the material to the application of three electric fields far from resonance with any optical transition (as described by Eq. 4): (i) A purely electronic contribution, due to the distortion of the electron clouds of atoms

---

The author is in the Department of Chemistry and European Laboratory for Non-Linear Spectroscopy, University of Florence, 50125 Florence, Italy.

and molecules. It is a practically instantaneous effect, which exists only for the duration of the excitation pulse. It is expressed in terms of the ensemble average of the hyperpolarizability $\langle \gamma_{ijkl} \rangle$. (ii) A nuclear contribution, due to the partial orientation of the molecules in the excitation field, is present whenever the molecules possess a nonisotropic polarizability. The corresponding contribution to the third-order polarizability is given by

$$R_{ijkl}(t) = \frac{iV}{2\hbar} \langle [\chi_{ij}^{(1)}(t), \chi_{kl}^{(1)}(0)] \rangle \qquad (10)$$

which represents the ensemble average of the time correlation function of the linear susceptibility $\chi_{ij}^{(1)}$ (t), strictly related to the molecular polarizability, where $\hbar = h/2\pi$ and h is Planck's constant, and V is the active volume. In other words, the intense excitation pulse modifies the random orientation distribution of the molecules, causing a partial alignment of the molecules in the direction of the electric field. This slightly out-of-equilibrium, uneven distribution of the molecular orientation is responsible for the setup of the transient birefringence. The spontaneous rotational motion of the molecules brings the system back to the isotropic equilibrium situation, in a time that is characteristic of the rotational dynamics of the molecules involved. By measurement of the intensity of the transmitted probe as a function of the delay time (see Eq. 8), the rotational relaxation time can be obtained directly.

This simple picture of the transient OKE, although evocative of the main aspects of the physical effect, is oversimplified. Both experimental evidence and theoretical predictions show that, at least in a short time range (typically 1 to 2 ps), other processes have to be taken into account. The first-order electric susceptibility $\chi_{ij}^{(1)}(t)$ that appears in Eq. 8 cannot, in general, be considered simply as the sum of the polarizabilities of the molecules of the sample. Other processes, essentially originating from the intermolecular interactions, may affect the sample susceptibility by producing a transient anisotropy resulting in additional contributions to the OKE signal. In addition, the molecular polarizability is modulated by the intramolecular vibrational motion. As a consequence, intermolecular collisions and molecular vibrations have to be considered as possible sources of optically induced birefringence. Of course these contributions can be observed only if a high time resolution is available, because the characteristic time of the originating processes is generally in the sub-picosecond range.

Works from the laboratories of Kenney-Wallace (3), Nelson (4), and McMorrow (5), who used very short (<100 fs) pulses in their experiments, clearly show the complex dynamics of pure liquids that OKE experiments can reveal in the short time domain. In summary, five contributions to the time-resolved OKE signal can be distinguished: (i) A purely electronic contribution, due to the molecular hyperpolarizability, gives an instantaneous response. (ii) An intermolecular "librational" contribution is originated by the librational motion of the molecules in the cage of the first neighbor molecules. Its decay is fast (typically <200 fs) due to the inhomogeneous dephasing by the liquid environment. (iii) An intramolecular vibrational "Raman" contribution decays with the dephasing time of the molecular vibrations (typically few hundreds of femtoseconds). (iv) A term originating from the intermolecular interactions is correlated to the density fluctuations and hence to the collision-induced anisotropy of the molecular polarizability. Its relaxation is governed by the lifetime of the local structure in the liquids, again few hundreds of femtoseconds. (v) There is also a rotational contribution, whose time scale can span a wide range of values, from a few picoseconds to several nanoseconds, depending on the molecular size and on the viscosity.

According to the Heisenberg uncertainty relation, very short pulses have broad transform-limited linewidths (up to several hundreds of inverse centimeters). Consequently, low-frequency molecular vibrations [contribution (iii) above] can be excited efficiently by stimulated Raman effect. Several experiments, like those by Nelson (4) represented in Fig. 2, that used the polarization grating technique revealed the oscillations in the OKE signal due to the coherently excited (iii) contribution. The molecular vibration is thus observed directly in the time domain, the period of the oscillations corresponding to that of the intramolecular vibrational mode. A damping of the oscillation is also clearly visible, with a time constant corresponding to the dephasing time of the vibration. The results of ultrafast transient birefringence and of frequency-domain Raman spectroscopy in the investigation of sub-picosecond dynamics of simple liquids are discussed in a recent paper (6), in which special attention is devoted to the separation of inter- and intramolecular vibrational contributions.

The implementation of optical heterodyne detection (OHD) (7) has been shown to be particularly useful in this kind of experiment. The OHD technique was used by McMorrow and Lottshaw in their investigation of the ultrafast dynamics of liquid acetonitrile (8). This technique consists of the coherent mixing at the detector of a local oscillator $\mathbf{E}_{LO}$ with the signal field $\mathbf{E}_S$; the detected signal thus has the form

$$S(\tau) = \int_{-\infty}^{\infty} dt \mathbf{E}_{LO}^{*}(t - \tau)\mathbf{E}_S(t - \tau)R(t) \qquad (11)$$

In addition to its high sensitivity and good signal-to-noise ratio, OHD has the advantage of measuring directly the material response function $R(t)$, instead of its second power, as in normal OKE (see Eq. 8). This measurement is specially relevant when $R(t)$ has an imaginary component (as is the case whenever resonances with stationary states of the system are involved in the process). In such a case the proper choice of the phase of the local oscillator allows the real and imaginary parts of $R(t)$ to be detected separately. The authors in (6) were thus able to identify the very fast nonexponentially decaying intermolecular vibrational contribution to the OKE signal (resonantly excited by stimulated Raman effect), superimposed on the slower rotational contribution.

The fine time resolution made possible by the use of very short pulses in the OKE is of great help in the identification of the

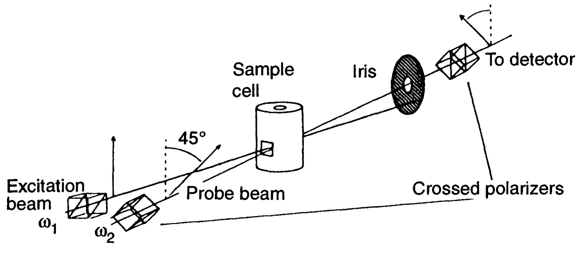

Fig. 1. Scheme of an OKE experiment. The probe pulse is polarized at 45° with respect to the excitation pulse. The birefringence induced in the sample opens the optical gate represented by the two crossed polarizers, and a fraction of the probe intensity reaches the detector.

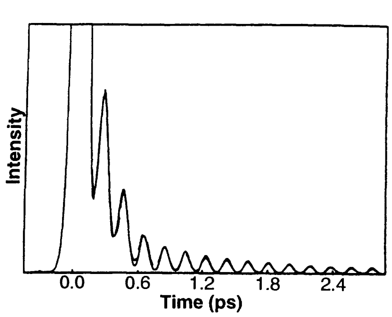

Fig. 2. When the duration of the pulses is shorter than the molecular vibrational period, the vibration itself can be excited impulsively. The time modulation that appears in the signal of liquid CH_2Br_2 corresponds to the frequency (173 cm^{-1}) of the Br bending vibration.

different contributions to the third-order susceptibility of the medium. This method has been used to study the nonlinear optical behavior of simple ionic solutions as a function of the concentration (9). For instance, Fig. 3A shows the different decay curves obtained for HNO_3 in water at different concentrations. From an accurate fit of the full set of curves it has been possible to characterize the different contributions to the signal: (i) an instantaneous electronic response; (ii) a fast ($\tau_1 = 700$ fs) relaxation, attributed to the collision-induced contribution of water; (iii) an intermediate process, with a time constant τ_2 of 2.2 ps, corresponding to the rotational relaxation of the individual NO_3^- ion; and (iv) a slow decay, whose time constant τ_3 increases with increasing concentration. In Fig. 3B the behavior of the two decay times corresponding to the above points (iii) and (iv) is shown. The increase of τ_3 with concentration is clear evidence of the cooperative nature of the associated process. The appearance of the τ_3 relaxation coincides with the disappearance of "free" water molecules: For concentrations higher than about 5 M, the NO_3^- ions "see" each other directly, thus setting up strongly correlated multi-ionic structures. In this sense, one can speak of the glassy nature of these highly concentrated solutions. A similar behavior was observed by transient OKE in molten $2[Ca(NO_3)_2]\cdot3[KNO_3]$ (*10*), a well-known glass-forming viscous liquid.

Clearly, most of the interest in the time-resolved OKE experiments is due to the possibility of obtaining direct information on the orientational dynamics of the molecules. When diluted solutions are used, the feasibility of the experiment is limited by the low signal from the solute molecules; this problem has been overcome in the case of β carotene in diluted (5×10^{-4} M) alkanes solution (*11*) by researchers who have taken advantage of the resonant amplification of the OKE. The idea is the excitation of the OKE effect, as usual, with pulses of wavelength far from the absorption band of the sample and the probing of the induced birefringence by means of pulses in resonance (or preresonance) with an electronic transition of the solute. With this method the birefringence is induced without involving any excited state of the molecule, whose finite lifetime could interfere with the detection of the decay of the OKE signal. On the other hand, the efficiency of the probing process is enhanced by the large increase of the molecular polarizability close to resonance. The time profile of the transient OKE signal for β carotene in dodecane ($\lambda_{exc} = 600$ nm, $\lambda_{probe} = 515$ nm, measured relaxation time $\tau_R = 215$ ps) is shown in Fig. 4A. Figure 4B illustrates the amplification effect due to the resonance effect of the probe pulse. In this case, the birefringence is probed with pulses of white light (covering the spectral range of 400 to 800 nm). The spectrum of the OKE signal follows closely the absorption profile of β carotene. Thanks to the resonant amplification of $\chi^{(3)}$, only the blue components of the probe pulse experience the weak birefringence induced in the diluted solution by the excitation pulse.

Not only in liquids has the molecular dynamics been studied by means of OKE experiments. Plastic crystals, for instance, are solids in which the molecules occupy fixed and symmetrically arranged positions in a lattice, as in normal crystals, but are allowed to change their orientation in an essentially random way by rotating around their center of mass. In the case of succinonitrile, for instance, the OKE experiments provided evidence for a complex

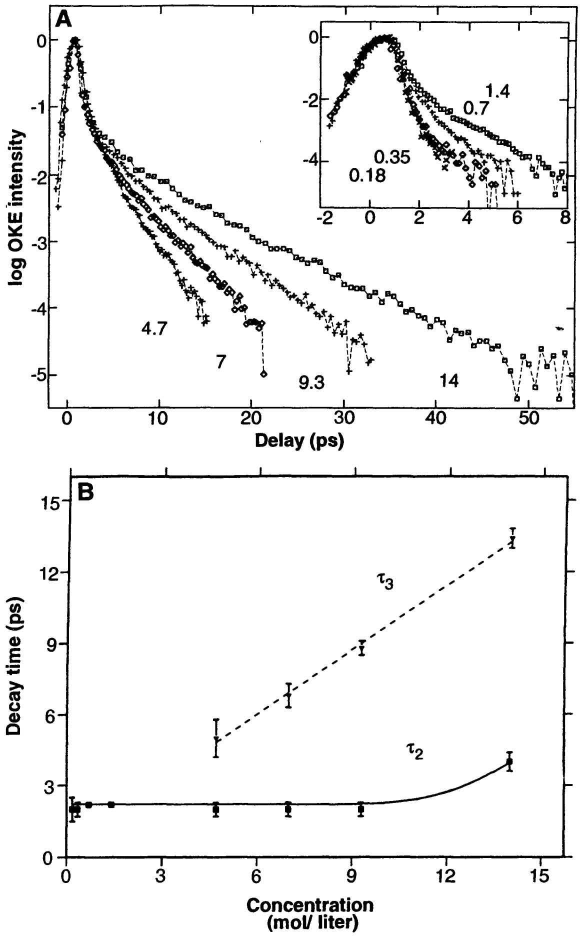

Fig. 3. (**A**) Optical Kerr effect decay profiles obtained for water solutions of HNO_3 of different concentrations. The appearance of a relatively slow relaxation is evident at high concentrations. The number by each trace is concentration in moles per liter. (**B**) Concentration dependence of τ_2 and τ_3 rotational relaxation times in HNO_3 solution.

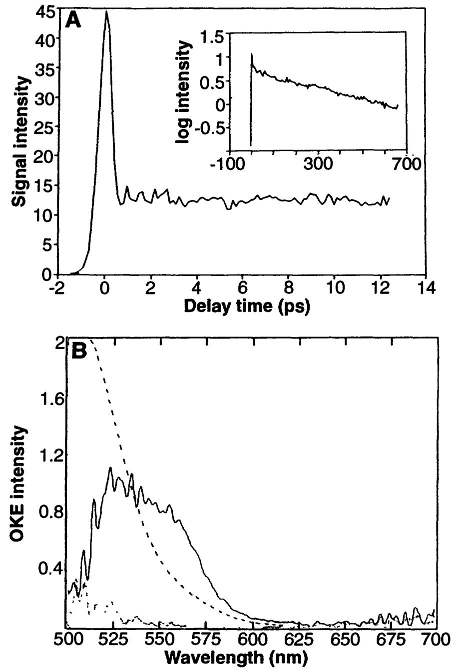

Fig. 4. (**A**) Optical Kerr effect signal decay in β carotene solution. The strong instantaneous electronic response and the delayed nuclear response are clearly visible. (**B**) Evidence for the resonance amplification effect in β carotene solution. If a white light pulse is used to probe the induced birefringence, only the blue part of it is efficiently depolarized, as a consequence of the resonant amplification of the nonlinear susceptibility. The dashed trace is the profile of the absorption band, and the full trace and the dotted trace are the spectra of the OKE signal of the solution and of the pure solvent, respectively. The calibrations are in arbitrary units.

orientational dynamics that involves both "external" and "internal" degrees of freedom of the flexible molecules, which show an equilibrium between the *gauche* and the *trans* conformations (*12*). Of the two relaxation times that characterize the decay of the OKE signal (Fig. 5A), the faster is associated with the "spinning" motion of the *trans* molecules (Fig. 5B). The slower relaxation process is instead dominated by the "tumbling" of the molecules in both conformations. The comparison with other experimental data and the results of a computer simulation both indicate that the two processes are essentially nondiffusive, involving long angular jumps from one orientation to the other, as expected for a strongly cooperative solid system.

The possibility of measuring dynamical effects over a very broad range of time scales (from 100 fs to tens of nanoseconds) is one of the most attractive features of OKE experiments. From this point of view, transient grating–detected OKE (also known as polarization grating) (*13, 14*) has been shown to be particularly useful. In this experiment, the excitation beam is split in two beams, which are crossed into the sample at an angle. The interference of the two pulses coincident in time and space induces in the sample a periodic spatial variation of the refractive index, which acts as a diffraction grating for the probe beam. The great advantage of this setup is that, by the proper choice of the polarization directions of the two excitation beams, of the probe beam, and of the final polarizer, it is possible to separate in the experiment the purely electronic contribution from the different nuclear terms. In the transient grating experiment performed by Fayer and colleagues on liquid biphenyl (*14*), the clean separation of the two different effects not only allowed the unambiguous distinction among the molecular contributions but also the measurement of the rise time of the nuclear term, corresponding to the inertial motion of the molecules under the effect of the torque exerted by the field of the dipoles induced in the molecules themselves by the laser pulses.

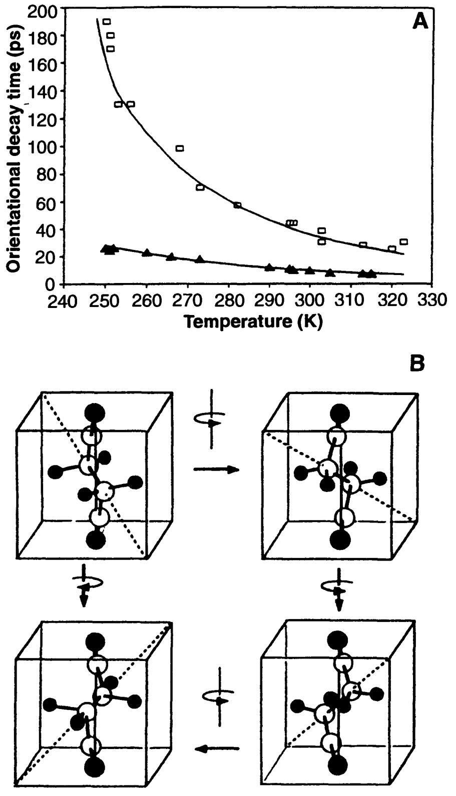

Fig. 5. (**A**) Temperature dependence of the two relaxation times observed in succinonitrile plastic crystal. (**B**) The *trans* molecules in the crystal unit cell can flip from one body diagonal to the other through a spinning motion around the long axis.

Experimental methods that are used to follow the molecular dynamics in condensed phases over different time scales is of special importance to the study of the critical processes that characterize the dynamics of molecular systems approaching a phase transition. The possibilities offered by the OKE experiment are illustrated by the results obtained on the liquid-solid transition of *P*-terphenyl (*15*) and *P*-quaterphenyl. Both molecules have the shape of an elongated cylinder. Together with fast rotation about the long axis, a much slower rotation about the short axis is expected to characterize the molecular dynamics in the liquid phase. The OKE experiments show a complex relaxation. For short delay times two contributions are recognized: a subpicosecond term originated by the vibrational excitation and a fast (2 to 5 ps, depending on the temperature) orientational relaxation corresponding to the rotation about the long molecular axis. By far the most intense contribution is that originated by the molecular rotation about the short axis; for temperatures lower than 570 K this contribution shows a clear biexponential decay (Fig. 6A). The shorter time constant follows the usual behavior of normal liquids also at temperatures close to the transition point T_c, whereas the longer time diverges approaching the solid phase (Fig. 6B). The data can be interpreted on the basis of the Landau–De Gennes (*16*) theory developed for the isotropic-nematic transition in liquid crystals. The "long" orientational relaxation time then diverges as a critical temperature T^* is approached, according to

$$\tau(T) \propto \frac{\eta(T)}{(T - T^*)} \qquad (12)$$

where η is the viscosity and T^* is a temperature slightly below that of the phase transition.

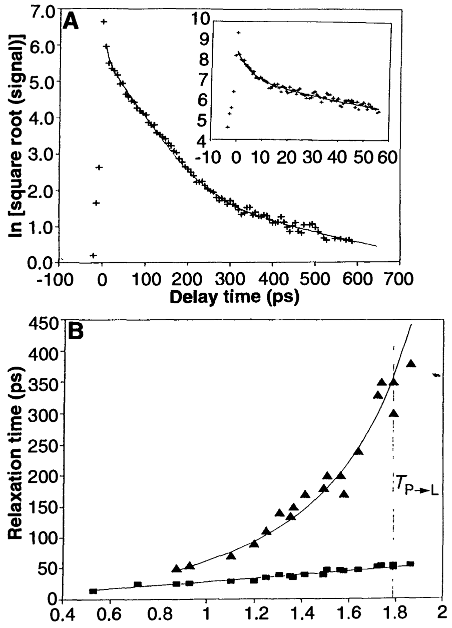

Fig. 6. (**A**) The square root of the OKE signal decay in *P*-terphenyl shows the biexponential nature of the relaxation on the long time scale. The insert illustrates the fast decay process characterizing the first few picoseconds of the relaxation. The calibration is in arbitrary units. (**B**) The two relaxation times show a different behavior with temperature: The slow process shows a clear diverging behavior approaching the phase transition, which is well reproduced by the Landau–de Gennes theory (solid trace). The transition temperature between plastic crystal and liquid ($T_{P \to L}$) is indicated.

The critical slowing of the rotational dynamics corresponds to the setting up of cooperative motions in the liquid due to the strong orientational correlation between neighbor molecules. In other words, the OKE experiment reveals the progressively increasing organization of the liquid in partially ordered local structures, whose size and lifetime grow substantially when the system is cooled toward the phase transition.

The OKE appears as a promising experimental tool in the investigation of processes involving molecular orientational dynamics in condensed phases. Many experiments performed up to now have shown that OKE can unveil some aspects of the molecular dynamics in liquids and solids that had not been observed with the use of other techniques, like Rayleigh and Raman light scattering or fluorescence depolarization. Although in principle the frequency-domain techniques can provide the same information, in many cases time-resolved OKE allows the detection of events that happen on a much broader range of time scales. The very fast relaxation times (up to less than 100 fs) measured by transient OKE correspond to extremely broad bands that can hardly be detected in the optical spectra. On the other hand, slowly relaxing processes (several nanoseconds) are easily observed in the time-domain experiments, whereas the corresponding bandwidths in the optical spectra are well below the accessible frequency resolution. The picture of molecular liquids, for instance, that emerges from the investigation by means of time-resolved techniques is in many cases more complex than expected. In this respect, the OKE and related time-domain experimental methods are of special interest to the study of critical phenomena, often characterized by very different time scales. The use of the time-resolved OKE technique will lead to substantial gains in the understanding of certain aspects of liquids and solids, such as the structure and dynamics of liquids, mostly in the proximity of phase transitions, where a high degree of molecular organization is likely to appear; the processes involved in the formation of glasses; and the intra- and intermolecular dynamics of liquid crystals.

One of the main problems encountered in this kind of investigation is the generally weak intensity of the nuclear signal (the one containing the dynamical information) with respect to the electronic contribution. The new solid-state laser systems that are now becoming available, providing short, intense pulses at a high repetition rate (typically 100 fs, 500 μJ per pulse at a repetition rate of several kilohertz), are expected to enlarge substantially the field of application of the technique.

REFERENCES

1. S. Kielich, *Acta Phys. Pol.* **30**, 683 (1966).
2. R. W. Hellwarth, *Prog. Quantum Electron.* **5**, 1 (1977).
3. D. McMorrow, W. T. Lottshaw, G. A. Kenney-Wallace, *IEEE J. Quantum Electron* **24**, 443 (1988).
4. Y. Yan and K. A. Nelson, *J. Chem. Phys.* **87**, 6240 (1987); S. Ruhman, A. G. Joly, B. Kohler, L. R. Williams, K. A. Nelson, *Rev. Phys. Appl.* **22**, 1987 (1717).
5. D. McMorrow and W. T. Lottshaw, *Chem. Phys. Lett.* **178**, 69 (1991).
6. M. Cho, M. Du, N. F. Scherer, G. R. Fleming, S. Mukamel, *J. Chem. Phys.* **99**, 2410 (1993).
7. G. L. Eesley, M. D. Levenson, W. M. Tolles, *IEEE J. Quantum Electron* **14**, 45 (1978).
8. D. McMorrow and W. T. Lottshaw, *J. Phys. Chem.* **95**, 10395 (1991).
9. I. Santa, P. Foggi, R. Righini, J. Williams, in preparation.
10. M. Ricci, P. Foggi, R. Righini, R. Torre, *J. Chem. Phys.* **98**, 4892 (1993).
11. P. Foggi, R. Righini, R. Torre, V. F. Kamalov, *Chem. Phys. Lett.* **193**, 23 (1992).
12. P. Foggi, R. Righini, R. Torre, L. Angeloni, S. Califano, *J. Chem. Phys.* **96**, 110 (1992).
13. J. Etchepare, G. Grillon, J. P. Chambaret, G. Hamoniaux, A. Orzag, *Opt. Commun.* **63**, 329 (1987).
14. F. D. Deeg, J. J. Stankus, S. R. Greenfield, V. J. Newell, M. D. Fayer, *J. Chem. Phys.* **90**, 6893 (1989).
15. R. Torre, I. Santa, R. Righini, *Chem. Phys. Lett.* **212**, 90 (1993).
16. P. G. de Gennes, *The Physics of Liquid Crystals, Fundamentals* (Springer, Berlin, 1988).

Active Optics, Adaptive Optics, and Laser Guide Stars

N. Hubin and L. Noethe

Optical astronomy is crucial to our understanding of the universe, but the capabilities of ground-based telescopes are severely limited by the effects of telescope errors and of the atmosphere on the passage of light. Recently, it has become possible to construct inbuilt corrective devices that can compensate for both types of degradations as observations are conducted. For full use of the newly emerged class of 8-meter telescopes, such active corrective capabilities, known as active and adaptive optics, are essential. Some physical limitations in the adaptive optics field can be overcome by artificially created reference stars, called laser guide stars. These new technologies have lately been applied with success to some medium and very large telescopes.

Since its invention 300 years ago, the astronomical telescope has evolved from a small, manually pointed device for visual observations to a large and sophisticated computer-controlled instrument by which information is collected electronically. Throughout this development, two parameters have been particularly important: the light-collecting power or diameter of the telescope (allowing the detection of fainter and more distant objects) and the angular resolution (that is, the sharpness of the image). For a perfect telescope used in a vacuum, resolution can be improved by increasing the telescope diameter. A plane wavefront from distant star (effectively at infinity) would be converted by the telescope into a perfectly spherical wavefront, forming the image, and the ultimate angular resolution achievable is called the diffraction limit.

In practice, however, both atmospheric and telescope errors (Fig. 1) distort the spherical wavefront, creating phase errors in the image-forming ray paths. Even if they were optically perfect, ground-based telescopes observing at visible wavelengths could not, because of atmospheric turbulence alone, achieve an angular resolution better than telescopes of 10- to 20-cm diameter. For a 4-m telescope, atmospheric distortion degrades the spatial resolution by more than one order of magnitude compared with the diffraction limit, and the intensity at the center of the star image is degraded by a factor of 100. The causes of this degradation are random spatial and temporal wavefront perturbations induced by turbulence in various layers of the atmosphere; one of the principal reasons for sending the Hubble Space Telescope into space was to avoid these degradations. In addition, the image quality is affected by permanent manufacturing errors and by long time scale–wavefront aberrations introduced by mechanical, thermal, and optical effects in the telescope, such as defocusing, decentering, or mirror deformations generated by support errors.

Until recently, the astronomical telescope has remained a "passive" instrument. Without any inbuilt corrective devices to improve the quality of star images during observation, the only possible adjustments are those performed off-line or during the daytime while the telescope is not in operation.

Although it was thought that atmospheric distortions could not be avoided, mechanical improvements have been made to minimize the negative effects of the telescope errors. Mirror figuring and polishing were improved, and stiffer structures and thicker mirrors are now used to avoid

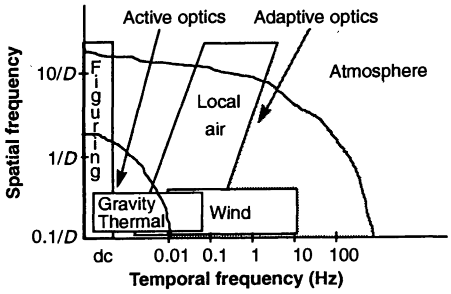

Fig. 1. Frequency domain of wavefront aberrations generated by various sources. The spatial frequency is measured in terms of *D*, the diameter of the telescope.

European Southern Observatory, Karl-Schwarzschild-Strasse 2, 85748 Garching, Federal Republic of Germany.